Journal of Inorganic and Organometallic Polymers and Materials
https://doi.org/10.1007/s10904-025-04062-2

RESEARCH

Synthesis of MIL-53(Al) Metal-Organic Framework from Aluminium-Lined Multi-Layered Packaging Materials and Polyethylene Terephthalate Bottles

Nokubongwa X. Dlamini[1] · Christophe A. Ndamyabera[1] · Mike Masukume[2] · Nicholas M. Musyoka[3] · Henrietta W. Langmi[1]

Received: 13 August 2025 / Accepted: 18 September 2025
© The Author(s) 2025

Abstract
A promising approach towards the synthesis of metal-organic frameworks (MOFs) is the use of precursors that can be extracted from waste materials found in landfills. In this work, we explore a combination of two waste materials for Al-based MOF synthesis. Aluminium sulphate was successfully derived from Poly-Al pellets obtained from multi-layered packaging materials. Terephthalic acid (BDC) was obtained from polyethylene terephthalate (PET) waste bottles. Both precursors were employed as metal and organic linker sources, respectively to synthesise MIL-53(Al). The results are compared with those of corresponding MOFs synthesised from commercial precursors and partly waste precursors. The study revealed that the structural properties of MIL-53(Al) synthesised from the two waste materials are comparable to those obtained when the MOF is synthesised using commercial sources of precursors or partly waste precursors. The MOFs were highly crystalline and stable up to 500°C. An improvement was observed in the surface area of the MOF when synthesised from complete waste (1588 m^2/g) as opposed to partly waste (1323 and 1197 m^2/g) and commercial precursors (1468 m^2/g). Although hydrogen adsorption capacity of the synthesised MOF materials was low at low pressures (<0.5 wt% at 1 bar and 77 K), attributable to the narrow pore form of MIL-53(Al), this work demonstrates an approach to waste management while producing high-value materials for various applications.

Keywords Metal-organic frameworks · Polyethylene terephthalate · Poly-Al pellets · MIL-53(Al)

1 Introduction

Metal-organic frameworks (MOFs) are crystalline adsorbent materials. They possess high surface area, which in combination with their high porosity makes them favourable for applications in catalysis [1, 2], drug delivery [3, 4] and gas separation and storage [5–7], among others. The combination of organic and inorganic units within MOFs allows for the incorporation of new functionalities and tunability of pore sizes, distinguishing them from other classes of porous materials [8, 9]. Although many MOFs structures have been reported, the stability of MOFs under various conditions still hinders their application [10]. Aluminium-based MOF, MIL-53(Al) has been extensively studied as one of the important MOFs owing to its good structural stability towards moisture, an important requirement for adsorbents used in industrial applications [11]. The structural stability of the MOF is attributed to strong coordination between

✉ Nicholas M. Musyoka
nicholas.musyoka@nottingham.edu.cn

✉ Henrietta W. Langmi
Henrietta.Langmi@up.ac.za

[1] Department of Chemistry, University of Pretoria, Private Bag X20, Hatfield 0028, South Africa

[2] Centre for Nanostructures and Advanced Materials, Chemical Cluster, Council for Scientific and Industrial Research (CSIR), Pretoria 0001, South Africa

[3] Nottingham Ningbo China Beacons of Excellence Research and Innovation Institute, University of Nottingham Ningbo China, Ningbo 315100, PR China

Published online: 04 November 2025

aluminium ions and terephthalic acid (1,4-benzenedicarboxylic acid; BDC) that is extensively used as a linker to construct many MOFs [12]. Despite the ligand's contribution to stabilization of the MOF, MIL-53(Al) is still a flexible MOF that undergoes a breathing phenomenon. This involves reversible transition of its pore size between a narrow pore (np) and large pore (lp) conformation in response to external stimuli such as pressure, temperature changes, and guest molecule adsorption [13]. Upon synthesis, the pores of MIL-53(Al) may be occupied by unreacted BDC ligands, which can be irreversibly expelled by heat treatment at temperatures above 270 °C, generating the lp form with empty pores. However, at room temperature, the pores adsorb water and transition to a np configuration as a result of hydrogen bonding interactions between water molecules and the framework's hydrophilic functional groups [14]. Similarly, studies on gas adsorption have displayed the flexibility of the MOF where reversible transition of the pore structure between the two configurations is induced at different temperatures and pressures [13, 15, 16].

The industrial production of MOFs is inhibited by many factors including the high cost of chemical feedstock, high energy consumption due to prolonged reaction times and the extensive use of organic solvent during synthesis [17]. To rectify this, the use of water as a green solvent or methods that eliminate solvent usage and reduce synthesis time have been investigated [18–20]. Waste valorisation has gained attention as a strategy for reducing the high cost of precursors needed for MOF synthesis [21, 22]. BDC has been retrieved from polyethylene terephthalate (PET) bottles, and utilised as an organic linker to synthesise MOFs like MOF-5, MIL-53 and UiO-66 [12, 23, 24]. PET materials are mass consumed and currently disposed of by dumping them in landfills, which negatively affects the environment due to poor biodegradability. Extracting terephthalic acid from waste bottles will not only reduce environmental pollution but will also lead to high-value PET-based materials production at an energy demand that is approximately half that needed for virgin resin [25].

Aluminium is a metal that is used extensively in the manufacturing industry to produce aeroplanes, automobiles, cables, beverage cans and foils, among others. To meet consumer needs for aluminium, large quantities of bauxite must be mined which generates a lot of waste. To alleviate the burden on the environment, aluminium can be recycled [26]. Aluminium household products, including beverage cans and foil, have been used as unconventional metal sources to synthesise MIL-59 (Al) and MIL-53(Al) MOFs [27, 28]. Coal fly ash has also been used as an unconventional feedstock in the synthesis of Al-fumarate (Al-Fum), MIL-53(Al) and their composites, which contributed in lowering the costs for MOF synthesis [29, 30]. Multi-layered packaging materials for liquid food (Tetra Pak) contain a significant amount of aluminium. These packaging materials are produced from laminating layers of stiff paperboard (75%), aluminium foil (5%) and 20% low-density polyethylene (LDPE) [31]. Owing to the complex structure of the packaging materials, their recycling is a challenge. Successful Tetra Pak recycling involves processing the entire material as is and technologies that depend on hydropulping as the initial step followed by separation of cellulose fibre from Poly-Al laminate [32].

Al-Fum MOF has been synthesised from aluminium sulphate derived from Poly-Al pellets obtained from the hydropulping of layered packaging materials [33]. Hence, this study employed a holistic approach to synthesise flexible MIL-53(Al) from the recycling of waste PET and Tetra Pak packaging materials, promoting a circular economy. The resulting MOF materials were compared to those synthesised from commercial precursors and partly waste which demonstrated a cost-effective way for MOF synthesis and the potential of MIL-53(Al) as a promising material for H_2 adsorption. To the best of our knowledge, there has been no report of the synthesis of MIL-53(Al) utilising both waste PET and Poly-Al from Tetra Pak packaging material as ligand and metal sources, respectively.

2 Experimental

2.1 Chemicals

Acetone (CH_3COCH_3, Radchem, 99.5%), aluminium sulphate octadecahydrate ($Al_2(SO_4)_3{\cdot}18H_2O$, Sigma-Aldrich, 97%), ethanol (CH_3CH_2OH, Radchem, 99.9%), terephthalic acid (BDC, Sigma-Aldrich, 98%), ethylene glycol ($HOCH_2CH_2OH$, Sigma-Aldrich, 99%), methanol (CH_3OH, Radchem, 99.8%), (N, N-dimethylformamide (DMF, Radchem, 99%), sodium aluminate ($NaAlO_2$, Sigma-Aldrich), anhydrous sodium hydroxide (NaOH, Sigma-Aldrich, 98%) and sulphuric acid (H_2SO_4, Sigma-Aldrich, 98%) were used as received. Deionised water was used to prepare solutions. Poly-Al pellets were obtained from a local hydropulping company while PET water bottles were salvaged from household waste and cleaned before use.

2.2 Terephthalic Acid Extraction

Waste PET bottles were depolymerized similarly to a previously reported method [34]. PET flakes (5 g) were placed in a hydrothermal synthesis reactor (autoclave) with ethylene glycol (5 mL) and deionized water. The autoclave was then heated to 210 °C and held there for 8 h. The reactor was cooled to ambient temperature. Centrifugation, two

consecutive washes with ethanol and drying at 100 °C for 24 h were done to obtain the product.

2.3 Sodium Aluminate Extraction

Poly-Al pellets obtained from the hydropulping of multi-layered packaging materials were mixed thoroughly with NaOH powder in 2:1 ratio of Poly-Al: NaOH. Transferring of the mixture into a crucible and heating it up to 550 °C in a muffle furnace was conducted. The furnace was held at a constant temperature for 1.5 h to obtain sodium aluminate (Na-Al) powder.

2.4 Conversion of Sodium Aluminate to Aluminium Hydroxide

Na-Al (5 g) was dissolved in deionized water while stirring. Ethanol (95% v/v) was slowly added while keeping the solution at room temperature and continuously stirred for 24 h. Suction filtration was employed to isolate the residue, which was purified with deionized water and vacuum dried at 60 °C overnight.

2.5 Aluminium Sulphate Synthesis

Aluminium hydroxide (5 g) was dissolved in 8 M sulphuric acid solution. The solution was refluxed for 2 h under continuous stirring. The resulting mixture was precipitated at room temperature. Then, the precipitate was washed with equivalent amounts of ethanol and acetone then vacuum dried at 60 °C.

2.6 MIL-53(Al) Synthesis

A hydrothermal method previously reported [35] with minor modifications was followed in MIL-53(Al) synthesis. A 0.5:1 ligand-to-metal ratio of BDC: Al was mixed ultrasonically in 50 mL deionized water. In the synthesis of MIL-53(Al) from commercial precursors, a precipitate began to form immediately. The reaction mixture was loaded into a Teflon-lined steel autoclave and heated at 150 °C for 24 h under autogenous pressure. The sediment was collected by centrifugation using a Thermo Scientific Labofuge 700 centrifuge. Thereafter, the product was refluxed in DMF for 24 h, followed by solvent exchange with methanol for 24 h. The product was then soaked in fresh methanol for a further 12 h, re-collected and dried overnight under vacuum at 60 °C.

2.7 Characterisation

Powder X-ray diffraction (PXRD) patterns of synthesised MIL-53(Al) powders and precursors were collected within a 3–70° range using a Bruker D2 Phaser benchtop diffractometer using Cu Kα radiation (λ = 1.5405 Å) at 2° s^{-1} scanning rate. FTIR spectra were obtained using a Brunker Alpha Fourier transform infrared (FTIR) spectrometer with platinum attenuated total reflectance (ATR) sampling accessory. A Zeiss 540 Ultra Field Emission Gun Scanning Electron microscopy (FEGSEM) was used to analyse the surface morphology of MIL-53(Al) samples where the samples were sprinkled on carbon tape and coated with carbon prior to analysis. The thermal stabilities of the MOFs were measured with a SDT Q600 V20.9 Build thermogravimetric analyser. A sample of a specified mass between 5 and 10 mg was heated to 800° at 20 °C.min^{-1}, under nitrogen gas flow of 20 mL.min^{-1}. Brunauer-Emmett-Teller (BET) surface areas and porosity of the materials were determined from nitrogen (N_2) sorption measurements at 77 K using a Micromeritics 3Flex high performance gas sorption analyser. The Non-Linear Density Functional Theory (NLDFT) was employed for calculation of pore size distribution. The Micromeritics 3Flex gas sorption analyser was also used for hydrogen (H_2) uptake measurements at 77 K and pressures up to 1 bar. All samples were degassed under vacuum at 120 °C preceding analysis.

3 Results and Discussion

3.1 Precursor Extraction

PET was hydrolysed into BDC by breaking down the ester bond in the PET [36]. Phase purity and crystallinity of the extracted BDC was confirmed by agreement between the XRD patterns of the commercial BDC and that derived from PET BDC (Fig. 1a). The O–H, C = O, C = C, C = H and C–H stretching bands at 2812, 1668, 1505, 1423 and 1278 cm^{-1}, respectively that were observed in the FTIR spectra (Fig. 1b), also confirmed the successful depolymerization of PET to obtain BDC. Admixing of Poly-Al pellets with NaOH at elevated temperatures resulted in the production of Na–Al. The diffraction pattern exhibited peaks like those of commercial Na-Al (Fig. 1c). Although a decrease in intensity was observed in the Poly-derived Na–Al XRD pattern, no additional peaks were present indicating phase purity. Therefore, Poly-Al derived Na–Al was deemed appropriate

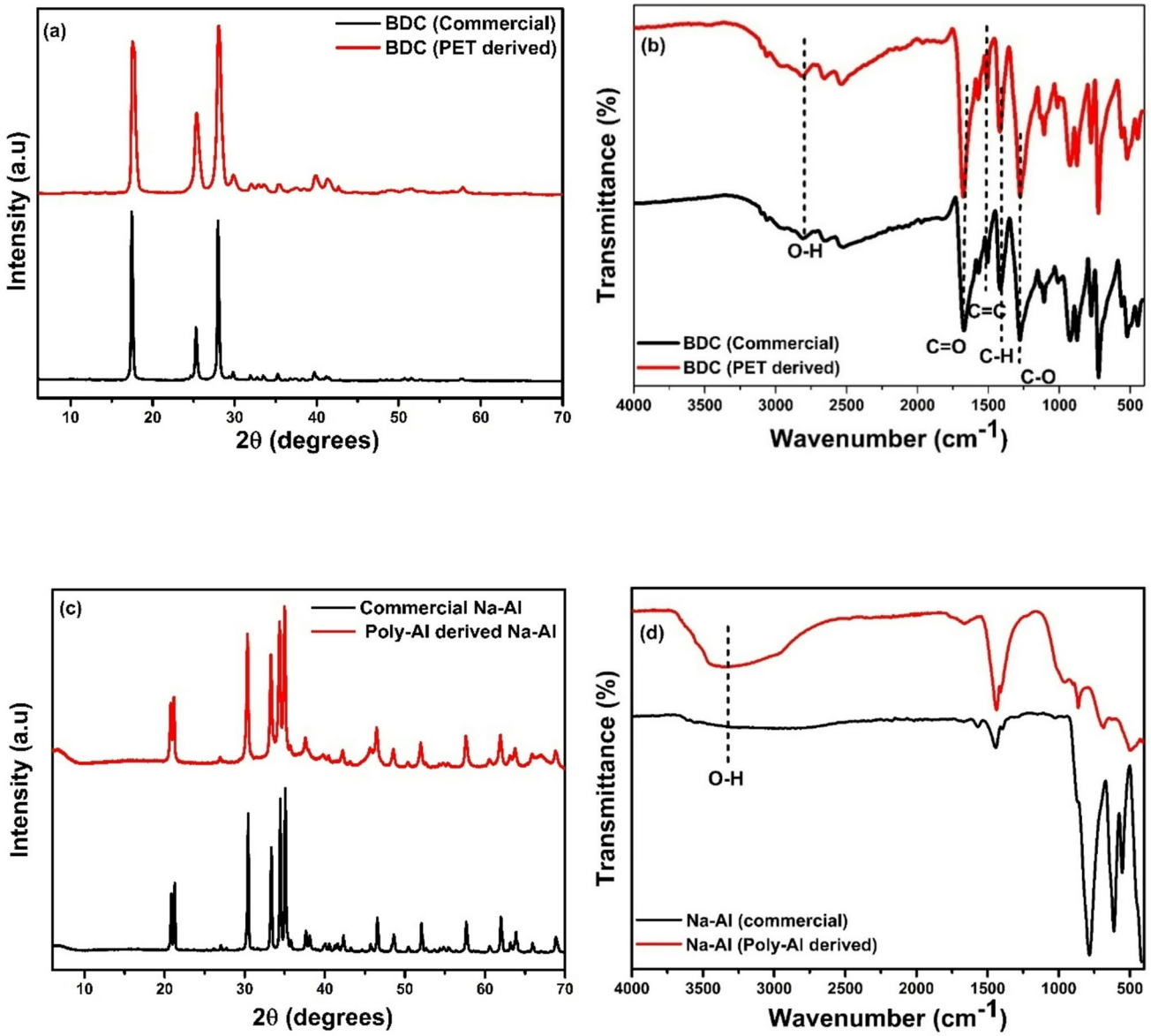

Fig. 1 **a** XRD patterns of BDC, **b** FTIR spectra of BDC, **c** XRD patterns of Na–Al and **d** FTIR spectra of Na–Al

to be converted to other Al products without further purification. The FTIR spectra (Fig. 1d) of Na–Al show a broad O–H stretch attributed to bound water thus indicating the formation of the hydrated form of Na–Al.

Water was added to Poly-Al derived Na–Al to transform it to Poly-Al derived aluminium hydroxide, $Al(OH)_3$. Figure 2a shows the XRD pattern of $Al(OH)_3$. Both XRD patterns resemble a mixture of the bayerite (α-$Al(OH)_3$) and gibbsite (γ-$Al(OH)_3$) polymorphs of $Al(OH)_3$. The enhanced peak intensities at 47.6° and 62.8° 2θ for Poly-Al derived $Al(OH)_3$ reveals dominance of the bayerite form [37, 38]. SEM was also used to identify $Al(OH)_3$ and Fig. 2b displays nanorods that self-assembled into fibre clusters as expected [39]. Shorter nanorods were observed for Poly-Al derived $Al(OH)_3$. The small difference observed in the morphology could be due to the dominance of the α-$Al(OH)_3$ in the poly-Al derived sample. $Al(OH)_3$ has been used previously for the preparation of MIL-53(Al), however, it was not the best candidate for industrial applications due to its insolubility in water [40].

Poly-Al derived aluminium sulphate hydrate was obtained from Poly-Al derived $Al(OH)_3$ and compared with the commercial standard. The XRD pattern (Fig. 2c) confirms the successful conversion of Poly-Al derived $Al(OH)_3$ to a hydrated aluminium sulphate, $Al_2(SO_4)_3$ salt of high crystallinity. A peak was observed at $2\theta < 10^o$ for both $Al_2(SO_4)_3$ samples, however, the peak intensity was very prominent for the commercial $Al_2(SO_4)_3$ with formula $(Al_2(SO_4)_3 \cdot 18H_2O$.

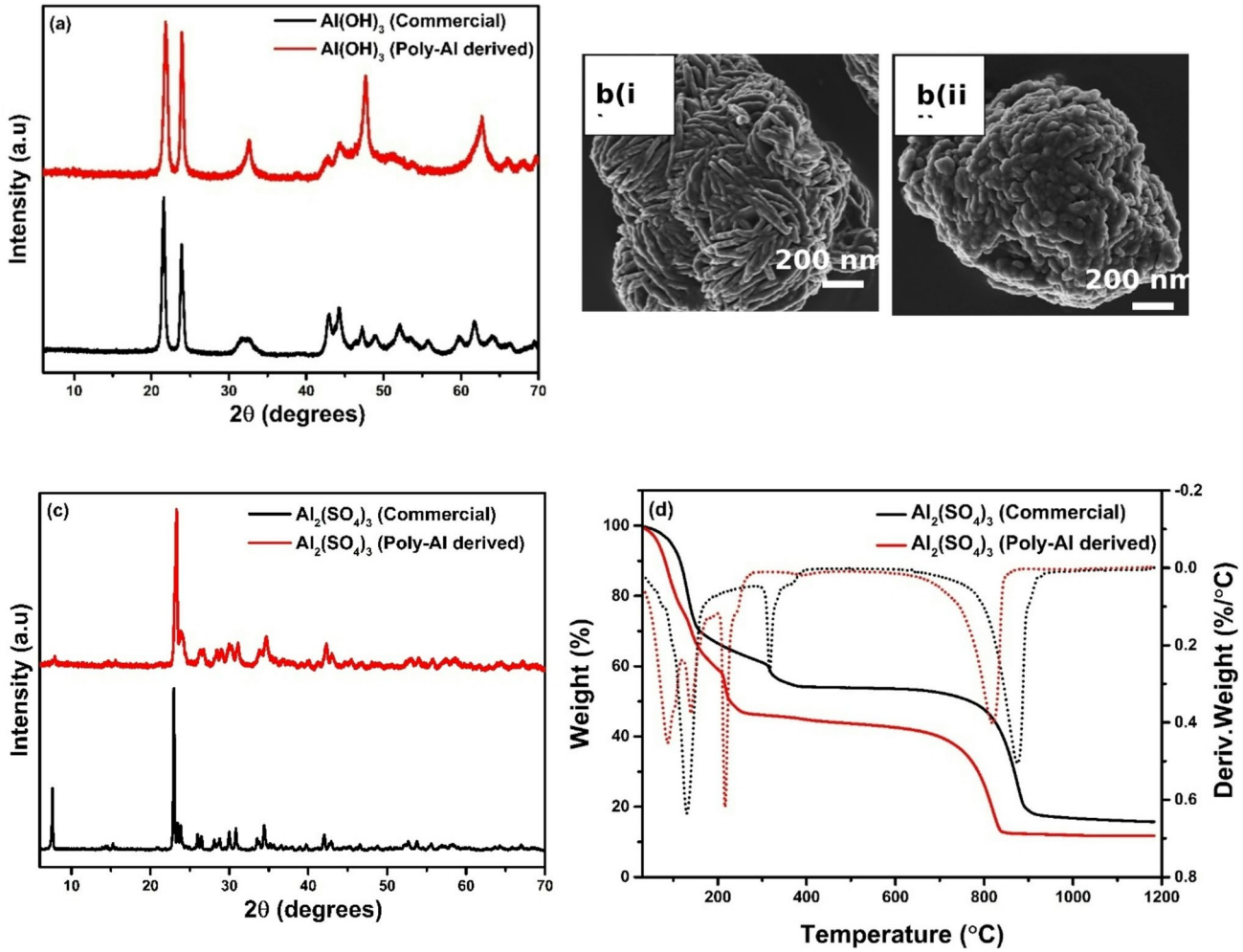

Fig. 2 **a** XRD patterns of $Al(OH)_3$, **b** SEM images of (i) commercial and (ii) Poly-Al derived $Al(OH)_3$, **c** XRD patterns of $Al_2(SO_4)_3$ and **d** TG (solid lines) and DTG (dotted lines) curves of $Al_2(SO_4)_3$

The low intensity of this peak and the slight shift of the peaks to the right for the Poly-Al derived $Al_2(SO_4)_3$ can be attributed to the formation of $Al_2(SO_4)_3.14H_2O$ similar to what was reported by Cao et al. [41]. Furthermore, the presence of a large number of water molecules in a compound will expand lattice spacings and induce diffraction at low 2θ angles analogous to what is seen in hydrated clays [42].

Thermogravimetric analysis (TGA) was employed in studying the decomposition profile of poly-derived aluminium sulphate hydrate and it revealed that it decomposes in four steps. Thermogram of Poly-Al derived $Al_2(SO_4)_3$ in Fig. 2d shows a 32% weight loss between 34 and 174 °C, corresponding to the DTG peak at 87 and 137 °C. This can be ascribed to the loss of free water present on the surface of $Al_2(SO_4)_3$. The second dehydration step was observed as the temperature increased between 204 and 239 °C, showing a 10% weight loss due to the loss of interlayer chemisorbed water between $Al_2(SO_4)_3$ molecules, corresponding to the DTG peak at 216 °C. The loss of SO_3 molecules leaves behind a residue of Al_2O_3 [43]. Based on a method reported by Lázaro [44], the % mass at a degradation step and % mass in residue were calculated and used to determine the theoretical mass loss between 600 and 950 °C. The calculated values were 40.4 and 36.0% for $Al_2(SO_4)_3{\cdot}14H_2O$ and $Al_2(SO_4)_3{\cdot}18H_2O$, respectively. From the TGA plots, the observed mass losses were 30.2 and 36.2% for Poly-Al derived $Al_2(SO_4)_3$ and commercial $Al_2(SO_4)_3$, respectively. The difference in the observed and expected mass loss for Poly-Al derived suggest the possibility of impurities though not evident from the XRD pattern (Fig. 2c).

3.2 Structural Properties of MIL-53(Al)

The Al-terephthalate MOF, MIL-53(Al) was successfully synthesised holistically from precursors extracted from waste materials. The XRD pattern of MIL-53(Al) prepared from waste precursors was compared to those of MIL-53(Al) powders prepared entirely from commercial

precursors or one waste derived precursor. Figure 3a shows that regardless of the precursor source, MIL-53(Al) exists in the np form which is expected when water is used in the synthesis of MIL-53(Al) without activating the MOF with heat at high temperatures [45, 46]. The patterns exhibit narrow, sharp peaks indicating high crystallinity as opposed to broad peaks that have been observed when DMF was used for synthesis, confirming that the solvent has an effect on the crystallinity of the frameworks as previously reported [47]. MIL-53(Al) was successfully synthesised in all cases with differences in peak intensities. However, for commercially derived MIL-53(Al) relatively broader peaks were observed suggesting a more nanocrystalline MOF. A diffraction peak was seen for all MOF samples at 12.3° 2θ, except for the PET derived sample. An additional peak at 24.6° 2θ can be seen in the diffraction pattern of commercially derived MIL-53(Al). These are not unexpected peaks as they have been reported and the absence or presence of these two peaks is influenced by the aluminium source used for MIL-53(Al) synthesis [45, 48, 49]. The two characteristic FTIR bands at 1592 and 1413 cm^{-1} are a result of C = O and C–O stretches, respectively (Fig. 3b). The absence of a broad O-H band between 2500 and 3500 cm^{-1} and the presence of an Al–O stretching vibration at 758 cm^{-1} on the FTIR spectra of all the MIL-53(Al) samples confirm successful coordination of the organic linker to the metal ion to form the frameworks [50]. These results reveal that MIL-53(Al) can indeed be synthesised wholly from Poly-Al and waste PET precursors.

Thermogravimetric analysis of the synthesised MIL-53(Al) samples shows a weight loss at temperatures up to 100 °C (Fig. 3c) due to loss of moisture within the pores of the MOFs [51]. The as-synthesised MOFs were refluxed in DMF to eliminate unreacted ligand from the pores of the frameworks. Although DMF was exchanged with methanol in the final washing steps the thermograms of the commercially derived and complete waste MIL-53(Al) exhibit

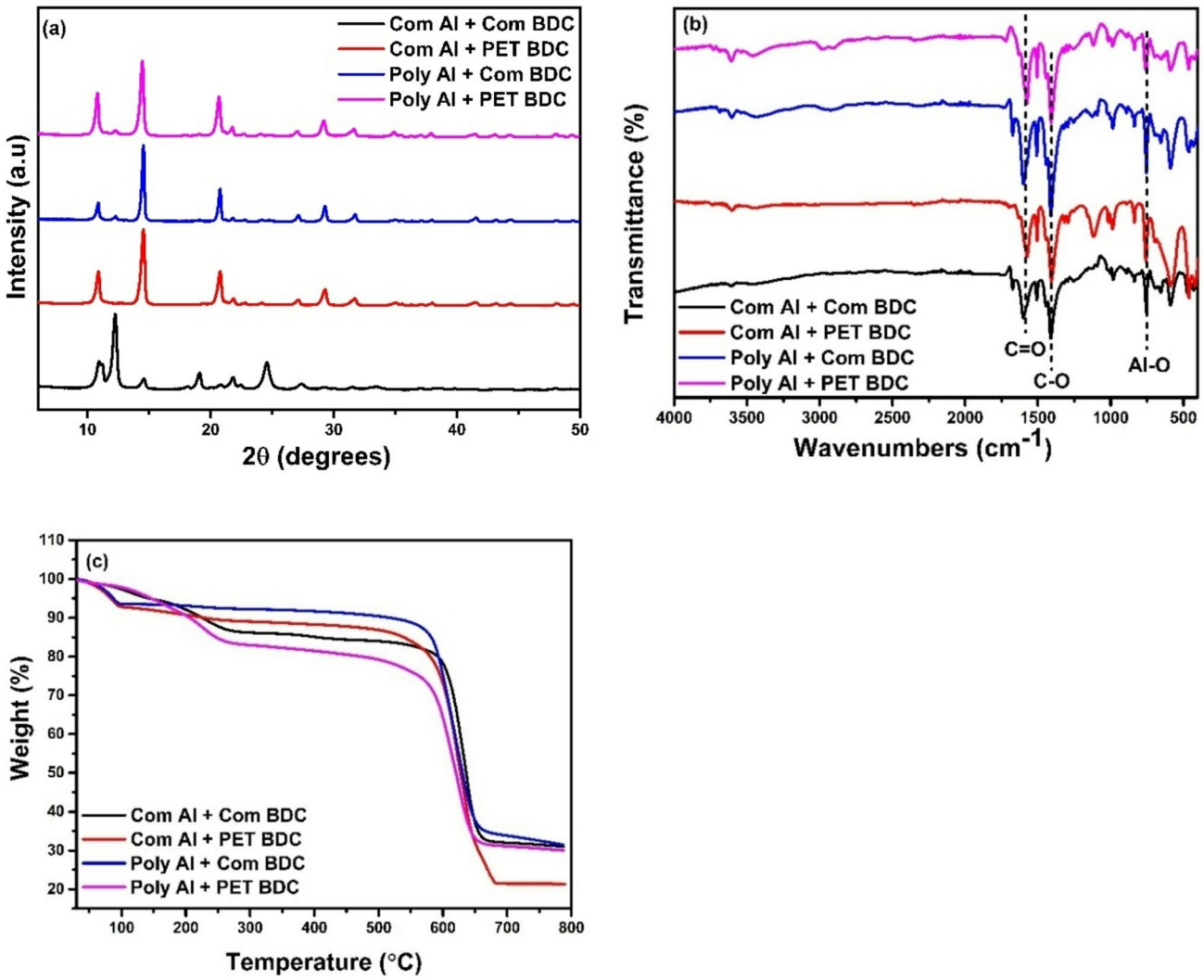

Fig. 3 **a** XRD patterns, **b** FTIR spectra and **c** TG curves of MIL-53(Al)

another weight loss between 100 and 260 °C which can be ascribed to loss of DMF molecules that were trapped in the pores of the frameworks. DMF molecules interact with hydroxyl groups of the inorganic network via hydrogen bonding [47, 52]. The MIL-53(Al) samples are stable up to 500 °C after which a rapid increase in weight loss occurs as the MOF structures collapsed due to the disintegration of coordinated terephthalic acid at high temperatures [52].

According to Loiseau et al. [14] the synthesised MOF structure belongs to MIL-53(Al) np, which is hydrated form of MIL-53(Al), $Al(OH)[O_2C–C_6H_4–CO_2].H_2O$. Following a similar method reported by Lázaro [44], the theoretical mass loss between 450 and 800 °C for MIL-53(Al), $Al(OH)[O_2C–C_6H_4–CO_2].H_2O$ is 46.1%. The observed mass losses for commercially derived, PET-derived, Poly-Al derived, and complete waste MIL-53(Al) were 51.6, 65.4, 59.7 and 48.4%, respectively. The higher values observed compared to the theoretical value might be due to impurities from the precursors, which could not be observed in the XRD patterns (Fig. 3a) or SEM images (Fig. 4). Several factors can also influence mass loss such as the presence of defects, specific framework stability, solvent used for synthesis, chosen heating rate and conditions used during the TGA experiment [53, 54].

The morphology of the MIL-53(Al) samples was investigated and SEM images (Fig. 4) revealed that the difference in precursor sources influences the morphology of the samples, which supports the observation from XRD patterns. As shown in Fig. 4a, relatively small uniformly distributed crystals of MOFs were formed for commercially derived MIL-53(Al). The immediate precipitation during the synthesis results in nanocrystalline MOF formation [55]. The PET-derived precursor led to elongated morphology (Fig. 4b). The influence of PET-derived BDC may not be evident in the diffraction pattern of MIL-53(Al), however, the presence of residual by-products from PET depolymerization can affect crystal growth like in PET derived UiO-66 [56]. Poly-Al derived precursor resulted in an aggregation (Fig. 4c) while complete waste derived MIL-53(Al) had large voids with elongated and agglomerated crystals (Fig. 4d) due to the synergy of both waste derived precursors.

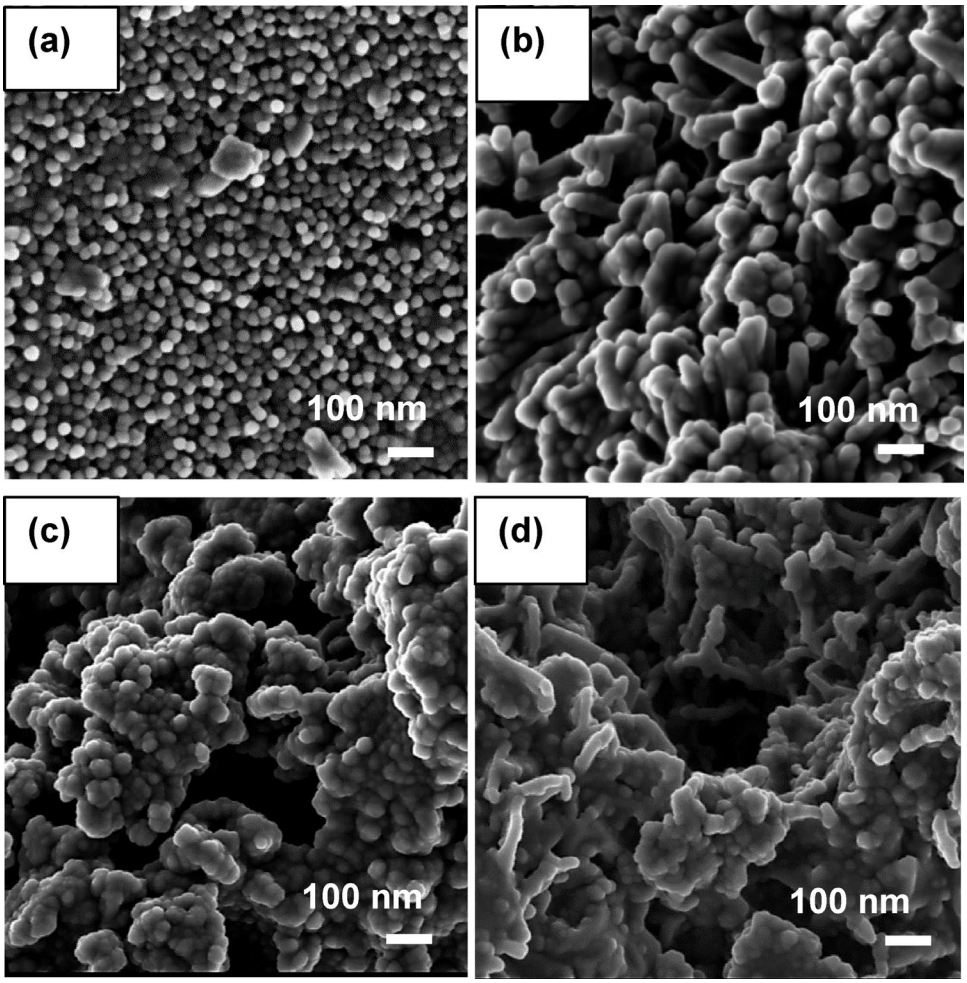

Fig. 4 SEM images of (**a**) Commercially derived, (**b**) PET derived, (**c**) Poly-Al derived and (**d**) Complete waste derived MIL-53(Al)

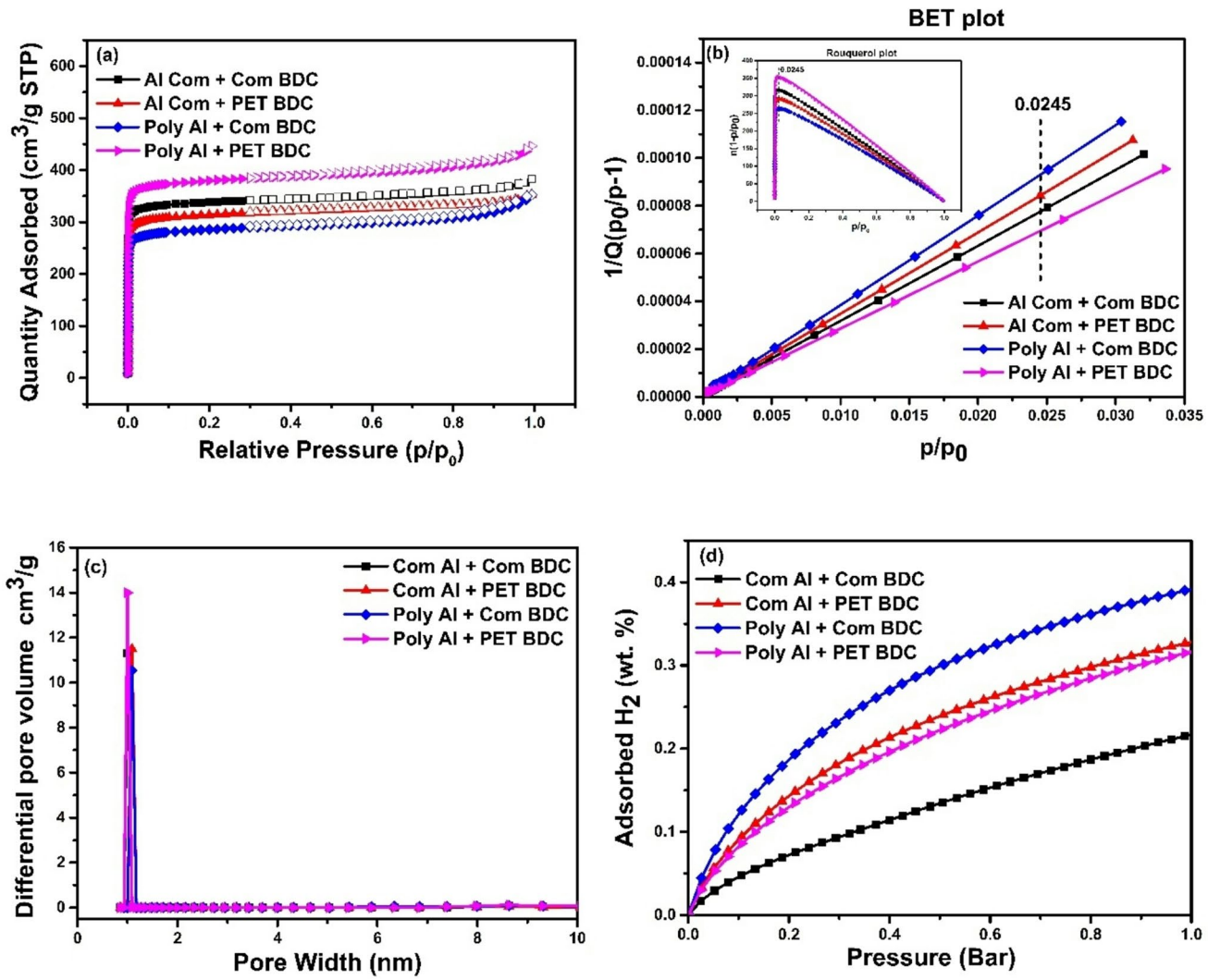

Fig. 5 **a** N_2 sorption isotherms (solid symbols for adsorption and empty symbols for desorption, **b** BET and Rouquerol plot **c** NLDFT pore size distribution curves and **d** H_2 adsorption isotherms at 77 K for MIL-53(Al)

3.3 Porosity and H_2 Uptake

N_2 adsorption measurements were performed on the synthesised MOFs, and the curves exhibit a type I isotherm, which is characteristic of microporous materials [11] (Fig. 5a). In this regard, there was a sharp increase in N_2 uptake at relative pressures below 0.05 (i.e. $p/p_0 < 0.05$) and no hysteresis loops were observed. BET surface area of the synthesised MIL-53(Al) samples were probed using BET analysis. The standard BET surface area measurement within a relative pressure range of 0.05–0.3 is better suited for materials containing mesopores [57]. For the synthesised samples, with dominant micropores, the BET relative pressure range is too broad and surpasses linearity of the BET plot. Therefore, BET linear range was corrected following Rouquerol criteria [57, 58] to determine the valid relative pressure range for specific BET surface area calculation for the microporous samples (Fig. 5b inset). Accordingly, Fig. 5b was plotted with a relative pressure range of 0.000321–0.0245 and positive C value used for the BET calculation. The obtained surface areas ranged from 1197 to 1588 m^2/g (Table 1). These surface areas are within the range of values reported in literature for MIL-53(Al) [35, 59]. It is notable that MIL-53(Al) derived from complete waste had the largest BET surface

Table 1 BET surface areas (SA_{BET}), pore volumes (V_{pore}) and diameters of MIL-53(Al)

Sample	SA_{BET} (m^2/g)	V_{pore} (cm^3/g)	Average pore diameter (nm)
Al Com + Com BDC	1468	0.57	1.00
Al Com + PET BDC	1323	0.53	1.09
Poly-Al + Com BDC	1197	0.51	1.09
Poly-Al + PET BDC	1588	0.66	1.00

area (1588 m^2/g) and pore volume (0.66 cm^3/g) revealing that the two waste materials had a synergistic effect in improving the surface area of MIL-53(Al) compared to MIL-53(Al) synthesised from commercial or partly waste precursors. The observed mass loss between 450 and 800 °C in the TGA (Fig. 3c) of complete waste MIL-53(Al) is the closest to the expected value, which corresponds to the highest surface area recorded. Furthermore, commercially derived MIL-53(Al) had the second lowest observed mass loss, which is in line with the second highest surface area. Therefore, in general, this indicates the impact impurities may have on the surface area of MOFs [23]. The surface area for each sample also correlates with the morphology, with the complete waste derived sample having a more open structure to allow for more gas sorption compared to a high aggregation exhibited by Poly-Al MIL-53(Al) (Fig. 4c) which reduces the surface area of the MOF [60]. Commercially derived MIL-53(Al) has small crystals and intercrystalline voids which enhances diffusion of gas molecules [61] contributing to a higher surface area observed compared to MIL-53(Al) derived from partly waste precursors.

Pore sizes below 2 nm were obtained, which further confirmed microporosity of the materials (Fig. 5c; Table 1) [62–64]. Low pressure H_2 uptake measurements were conducted at 77 K and the results are presented in Fig. 5d. The H_2 uptake values were in the range of 0.22 to 0.39 wt% and did not reach saturation at 1 bar. The hydrogen uptake capacities obtained at the experimental conditions of 1 bar and 77 K, are in line with the results obtained by Kim et al. under the same conditions [13]. H_2 uptake did not follow the same trend as the BET surface area. The commercially derived MIL-53(Al) shows the lowest H_2 uptake. Besides surface area, hydrogen uptake is influenced by other factors such as pore geometry, microporosity (intra- and intercrystalline pore) and pore flexibility for breathing MOFs which creates differences in H_2 uptake in as-synthesised samples [65–68]. Kim et al. showed that an increase in pressure induced the breathing effect of MIL-53(Al) changing its pore conformation from np to lp phase [13]. An increase in H_2 adsorption for the lp form at 77 K was reported from 3 bar with up to 4 wt% H_2 uptake at higher pressures [13]. This provides evidence that higher hydrogen adsorption capacities can be obtained using the synthesised materials with exposure to suitable temperature and pressure, owing to the structural flexibility of MIL-53(Al). Accordingly, one possible reason for the low uptake of H_2 for the commercially derived sample might also be its different breathing effect under the specified temperature and pressure conditions. This could arise from the structure and morphology of the commercially derived sample as shown in Figs. 3a and 4c, respectively in comparison to the other samples, which closely resemble each other.

4 Conclusion

This work demonstrates the successful conversion of waste PET bottles and Poly-Al to an Al-based MOF i.e. MIL-53(Al). The purity of the extracted BDC ligand from BET bottles was confirmed using XRD and FTIR. In addition to these techniques, SEM and TGA were used to confirm the successful extraction of Na-Al from Poly-Al pellets that was converted to $Al(OH)_3$ with dominant bayerite phase. The obtained $Al(OH)_3$ was then converted to $Al_2(SO_4)_3$. The properties of Poly-Al derived $Al_2(SO_4)_3$ corresponded to their commercial counterparts although reduced thermal stability and purity were observed for Poly-Al derived $Al_2(SO_4)_3$. MIL-53(Al) was successfully synthesised using water as a green solvent. The use of alternative feedstock did not compromise the crystallinity of MIL-53(Al). The observed mass losses between 450 and 800 °C for the synthesised MIL-53(Al) from TGA are higher than the expected value due to impurities from the precursors, which could not be observed in the XRD patterns or SEM images. The materials displayed high surface areas, and type I N_2 isotherms with no hysteresis loops were observed in accordance with results attained in literature. There was a correlation between surface area and morphology. The morphology exhibited by the complete waste derived MOF allowed for more N_2 gas adsorption as confirmed by the pore volume. The synthesised MIL-53(Al) adsorbed small amounts of hydrogen at 77 K and 1 bar due to their np structure. Future studies will involve exposing the materials to hydrogen at pressures up to 100 bar to enhance H_2 uptake by taking advantage of the breathing nature of the materials. This waste valorisation approach may be explored to synthesise other Poly-Al derived MOFs.

Acknowledgements MM and HWL acknowledge financial support from MAST3RBoost project funded by the European Union (Call HORIZON-CL4-2021-RESILIENCE-01, Grant Agreement No: 101058574). NMM acknowledges financial support from Nottingham Ningbo China Beacons of Excellence Research and Innovation Institute. HWL appreciates the South African Research Chairs Initiative (SARChI, Grant No: 2090155358) of the Department of Science, Technology and Innovation, and the National Research Foundation (NRF), and the NRF CPRR funding stream (Grant No: 0215586378).

Author Contributions Nokubongwa X. Dlamini: Investigation, methodology, validation, formal analysis, visualization, writing – original draft. Christophe A. Ndamyabera: Formal analysis, project administration, writing – review & editing. Mike Masukume: methodology, resources, writing – review & editing. Nicholas M. Musyoka: Conceptualization, methodology, supervision, funding acquisition, resources, writing – review & editing. Henrietta W. Langmi: Conceptualization, supervision, funding acquisition, methodology, project administration, resources, writing –review & editing.

Funding Open access funding provided by University of Pretoria. Financial support was received from MAST3RBoost project funded by the European Union (Call HORIZON-CL4-2021-RESILIENCE-01, Grant Agreement No: 101058574), the South African Research Chairs Initiative (SARChI, Grant No: 2090155358) of the Department of Science, Technology and Innovation, and the National Research Foundation (NRF), and the NRF CPRR funding stream (Grant No: 0215586378).

Data Availability The experimental data that supports the findings of this study will be available on request.

Declarations

Competing Interests The authors declare no competing interests.

Open Access This article is licensed under a Creative Commons Attribution 4.0 International License, which permits use, sharing, adaptation, distribution and reproduction in any medium or format, as long as you give appropriate credit to the original author(s) and the source, provide a link to the Creative Commons licence, and indicate if changes were made. The images or other third party material in this article are included in the article's Creative Commons licence, unless indicated otherwise in a credit line to the material. If material is not included in the article's Creative Commons licence and your intended use is not permitted by statutory regulation or exceeds the permitted use, you will need to obtain permission directly from the copyright holder. To view a copy of this licence, visit http://creativecommons.org/licenses/by/4.0/.

References

1. T.N. Tu, S.A. Khalate, K. Chang, J. Kim, Ship-in-a-bottle entrapment of biomolecules in MOF-based xerogel monoliths for high-performance electrochemical hydrogen evolution. J. Mater. Chem. A **12**, 7622–7630 (2024)
2. T. Marso, C. Kalpage, M. Udugala-Ganehenege, Application of chromium and cobalt terephthalate metal organic frameworks as catalysts for the production of biodiesel from *Calophyllum inophyllum* oil in high yield under mild conditions. J. Inorg. Organomet. Polym. Mater. **30**, 1243–1265 (2020)
3. A. Sharma, A. Thakur, Synthesis, characterization and in vitro drug delivery applications of a tin-based metal–organic framework. J. Inorg. Organomet. Polym. Mater. **35**, 2597–2611 (2025)
4. A. Golmohamadpour, B. Bahramian, A. Shafiee, L. Ma'mani, Slow released delivery of alendronate using β-cyclodextrine modified Fe–MOF encapsulated porous hydroxyapatite. J. Inorg. Organomet. Polym. Mater. **28**, 1991–2000 (2018)
5. T.N. Tu, P.N. Nguyen, H.T. Kwon, J. Kim, Macroporous MOF beads constructed from intergrown MOF nanoparticles for enhancing CO2 separation. Chem. Eng. J. (2025). https://doi.org/10.1016/j.cej.2025.164997
6. T.N. Tu, H.T. Kwon, M. Scheer, J. Kim, High toluene uptake at a trace concentration in a novel gallium-based metal–organic framework. J. Mater. Chem. A **13**, 9479–9485 (2025)
7. T.N. Tu, Y. Shin, S.A. Khalate, K. Chang, H.T. Kwon, J. Kim, Meso/macropore emerging from MOF granulation for enhancing performance in the Xe/Kr separation. Sep. Purif. Technol. **343**, 127128 (2024)
8. H.W. Langmi, J. Ren, B. North, M. Mathe, D. Bessarabov, Hydrogen storage in metal-organic frameworks: a review. Electrochim. Acta. **128**, 368–392 (2014)
9. R.M. Abdelhameed, M. Taha, H. Abdel-Gawad, B. Hegazi, Amino-functionalized Al-MIL-53 for dimethoate pesticide removal from wastewater and their intermolecular interactions. J. Mol. Liq. **327**, 114852 (2021)
10. L. Jiao, J.Y.R. Seow, W.S. Skinner, Z.U. Wang, H.-L. Jiang, Metal–organic frameworks: structures and functional applications. Mater. Today **27**, 43–68 (2019)
11. X. Qian, B. Yadian, R. Wu, Y. Long, K. Zhou, B. Zhu, Y. Huang, Structure stability of metal-organic framework MIL-53 (Al) in aqueous solutions. Int. J. Hydrogen Energy **38**, 16710–16715 (2013)
12. D. Villarroel-Rocha, M.C. Bernini, J.J. Arroyo-Gómez, J. Villarroel-Rocha, K. Sapag, Synthesis of MOF-5 using terephthalic acid as a ligand obtained from polyethylene terephthalate (PET) waste and its test in CO_2 adsorption. Braz. J. Chem. Eng. **39**, 949–959 (2022)
13. J.Y. Kim, L. Zhang, R. Balderas-Xicohténcatl, J. Park, M. Hirscher, H.R. Moon, H. Oh, Selective hydrogen isotope separation via breathing transition in MIL-53 (Al). J. Am. Chem. Soc. **139**, 17743–17746 (2017)
14. T. Loiseau, C. Serre, C. Huguenard, G. Fink, F. Taulelle, M. Henry, T. Bataille, G. Férey, A rationale for the large breathing of the porous aluminum terephthalate (MIL-53) upon hydration. Chem. Eur. J. **10**, 1373–1382 (2004)
15. S. Tomar, V. Singh, Review on synthesis and application of MIL-53. Mater. Today Proc. **43**, 3291–3296 (2021)
16. A. Boutin, M.-A. Springuel-Huet, A. Nossov, A. Gedeon, T. Loiseau, C. Volkringer, G. Férey, F.-X. Coudert, A.H. Fuchs, Breathing transitions in MIL-53 (Al) metal-organic framework upon Xenon adsorption. Angew. Chem. Int. Ed. **48**, 8314–8317 (2009)
17. W. Chai, Y. Shen, J. Wang, G. Zhang, Applications of metal-organic framework materials. J. Phys. Conf. Ser. (2022). https://doi.org/10.1088/1742-6596/2194/1/012014
18. W. Dong, X. Liu, W. Shi, Y. Huang, Metal–organic framework MIL-53 (Fe): facile microwave-assisted synthesis and use as a highly active peroxidase mimetic for glucose biosensing. RSC Adv. **5**, 17451–17457 (2015)
19. J. Beamish-Cook, K. Shankland, C.A. Murray, P. Vaqueiro, Insights into the mechanochemical synthesis of MOF-74. Cryst. Growth Des. **21**, 3047–3055 (2021)
20. D.A. Cabrera-Munguia, M.I. León-Campos, J.A. Claudio-Rizo, D.A. Solís-Casados, T.E. Flores-Guia, Cano Salazar, potential biomedical application of a new MOF based on a derived PET: synthesis and characterization. Bull. Mater. Sci. **44**, 1–9 (2021)
21. G.R. van Niekerk, H.W. Langmi, Modulator-Free green synthesis of the Calcium-Terephthalate Metal-Organic framework derived from waste eggshells. Polyhedron Polyhedron. **245**, 116618 (2023)
22. N.T. Mthembu, X. Dyosiba, H.W. Langmi, N.M. Musyoka, Holistic strategy for green synthesis of Fe-Mil-101 Mof from acid mine drainage and polyethylene terephthalate waste. SSRN (2024). https://doi.org/10.2139/ssrn.4742870
23. X. Dyosiba, J. Ren, N.M. Musyoka, H.W. Langmi, M. Mathe, M.S. Onyango, Feasibility of varied polyethylene terephthalate wastes as a linker source in metal–organic framework UiO-66 (Zr) synthesis. Ind. Eng. Chem. Res. **58**, 17010–17016 (2019)
24. S.-H. Lo, D.S. Raja, C.-W. Chen, Y.-H. Kang, J.-J. Chen, C.-H. Lin, Waste polyethylene terephthalate (PET) materials as sustainable precursors for the synthesis of nanoporous MOFs, MIL-47, MIL-53 (Cr, Al, Ga) and MIL-101 (Cr). Dalton Trans. **45**, 9565–9573 (2016)
25. X. Dyosiba, J. Ren, N.M. Musyoka, H.W. Langmi, M. Mathe, M.S. Onyango, Preparation of value-added metal-organic frameworks (MOFs) using waste PET bottles as source of acid linker. Sustain. Mater. Technol. **10**, 10–13 (2016)

26. S. Al-Busafi, Green preparation of aluminum-based metal-organic framework (Al-MOF) from waste plastic bottles and waste aluminum scraps. Sultan Qaboos Univ. J. Sci. [SQUJS] **26**, 98–106 (2021)
27. W. Liu, T. Niu, J. Yang, Y. Wang, S. Hu, Y. Dong, H. Xu, Preparation of micron-sized alumina powders from aluminium beverage can by means of sol–gel process. Micro Nano Lett. **6**, 852–854 (2011)
28. J.N. Joshi, C.M. Moran, H.P. Feininger, J.M. Dow, K.S. Walton, Household aluminum products as insoluble precursors for directed growth of metal–organic frameworks. Cryst. Growth Des. **19**, 5097–5104 (2019)
29. N. Yuan, X. Zhang, A. Zhao, K. Tan, Y. Cui, High-alumina fly ash as sustainable aluminum sources for the in situ preparation of Al-based eco-MOFs. Colloids Surf. A Physicochem. Eng. Asp. **640**, 128421 (2022)
30. K.M. Rambau, N.M. Musyoka, R. Panek, W. Franus, M. Wdowin, N. Manyala, Preparation of coal fly ash derived metal organic frameworks and their carbon derivatives. Mater. Today Commun. **27**, 102433 (2021)
31. I. Georgiopoulou, G.D. Pappa, S.N. Vouyiouka, K. Magoulas, Recycling of post-consumer multilayer tetra Pak® packaging with the selective dissolution-precipitation process. Resour. Conserv. Recycling **165**, 105268 (2021)
32. J. Zawadiak, S. Wojciechowski, T. Piotrowski, A. Krypa, Tetra pak recycling–current trends and new developments. Am. J. Chem. Eng. **5**, 37–42 (2017)
33. N.M. Musyoka, J. Ren, Recycling or processing of layered packaging materials. (WIPO, (ICT) 2020). https://patents.google.com/patent/WO2020095219A1/en. Accessed 29 July 2022
34. J. Ren, X. Dyosiba, N.M. Musyoka, H.W. Langmi, B.C. North, M. Mathe, M.S. Onyango, Green synthesis of chromium-based metal-organic framework (Cr-MOF) from waste polyethylene terephthalate (PET) bottles for hydrogen storage applications. Int. J. Hydrogen Energy. **41**, 18141–18146 (2016)
35. A. Taheri, E.G. Babakhani, J. Towfighi, Study of synthesis parameters of MIL-53 (Al) using experimental design methodology for CO_2/CH_4 separation. Adsorpt. Sci. Technol. **36**, 247–269 (2018)
36. F. Cao, L. Wang, R. Zheng, L. Guo, Y. Chen, X. Qian, Research and progress of chemical depolymerization of waste PET and high-value application of its depolymerization products. RSC Adv. **12**, 31564–31576 (2022)
37. S. Shayanfar, V. Aghazadeh, A. Saravari, P. Hasanpour, Aluminum hydroxide crystallization from aluminate solution using carbon dioxide gas: effect of temperature and time. J. Cryst. Growth. **496**, 1–9 (2018)
38. H. Zhang, X. Zhang, T.R. Graham, C.I. Pearce, H. Hlushko, J.A. LaVerne, L. Liu, S. Wang, S. Zheng, Y. Zhang, Crystallization and phase transformations of aluminum (oxy) hydroxide polymorphs in caustic aqueous solution. Inorg. Chem. **60**, 9820–9832 (2021)
39. T.S. Chang, J.H. Na, C.Y. Jung, S.M. Koo, An easy one-pot synthesis of structurally controlled aluminum hydroxide particles from an aqueous sodium aluminate solution. J. Ceram. Process. Res. **10**, 832–839 (2009)
40. Z. Li, Y. Wu, J. Li, Y. Zhang, X. Zou, F. Li, The metal–organic framework MIL-53 (Al) constructed from multiple metal sources: alumina, aluminum hydroxide, and boehmite. Chem. Eur. J. **21**, 6913–6920 (2015)
41. H. Cao, J. Chen, Z. Ling, Laboratory synthesis and spectroscopic studies of hydrated Al-sulfates relevant to Mars. Icarus. **333**, 283–293 (2019)
42. E. Ferrage, B. Lanson, N. Malikova, A. Plançon, B.A. Sakharov, V.A. Drits, New insights on the distribution of interlayer water in bi-hydrated smectite from X-ray diffraction profile modeling of 00 l reflections. Chem. Mater. **17**, 3499–3512 (2005)
43. G. Zheng, J. Xia, Z. Chen, J. Yang, C. Liu, *Study on kinetics of the pyrolysis process of aluminum sulfate, phosphorus, sulfur, and silicon and the related elements* (Taylor & Francis, NY, 2019). https://doi.org/10.1080/10426507.2019.1686377
44. I.A. Lázaro, A comprehensive thermogravimetric analysis multifaceted method for the exact determination of the composition of multifunctional metal-organic framework materials. Eur. J. Inorg. Chem. **45**, 4284–4294 (2020)
45. N. Ahadi, S. Askari, A. Fouladitajar, I. Akbari, Facile synthesis of hierarchically structured MIL-53 (Al) with superior properties using an environmentally-friendly ultrasonic method for separating lead ions from aqueous solutions. Sci. Rep. **12**, 2649 (2022)
46. J. Liu, F. Zhang, X. Zou, G. Yu, N. Zhao, S. Fan, G. Zhu, Environmentally friendly synthesis of highly hydrophobic and stable MIL-53 MOF nanomaterials. Chem. Commun. **49**, 7430–7432 (2013)
47. W.P. Mounfield III., K.S. Walton, Effect of synthesis solvent on the breathing behavior of MIL-53 (Al). J. Colloid Interface Sci. **447**, 33–39 (2015)
48. H.L. Choi, H. Yang, J. Woo, J.-H. Mun, T.-H. Bae, Upcycling PET waste into high-performance metal–organic frameworks: sustainable synthesis of MIL-53 (Al) for gas separation and storage. Korean J. Chem. Eng. (2025). https://doi.org/10.1007/s11814-025-00538-6
49. D. Panda, S. Patra, M.K. Awasthi, S.K. Singh, Lab cooked MOF for CO_2 capture: a sustainable solution to waste management. J. Chem. Educ. **97**, 1101–1108 (2020)
50. E. Moumen, L. Bazzi, S.E. Hankari, Aluminum-fumarate based MOF: a promising environmentally friendly adsorbent for the removal of phosphate. Process Saf. Environ. Prot. **160**, 502–512 (2022)
51. P. Mishra, H.P. Uppara, B. Mandal, S. Gumma, Adsorption and separation of carbon dioxide using MIL-53 (Al) metal-organic framework. Ind. Eng. Chem. Res. **53**, 19747–19753 (2014)
52. C. Serre, F. Millange, C. Thouvenot, M. Noguès, G. Marsolier, D. Louër, G. Férey, Very large breathing effect in the first nanoporous chromium (III)-Based solids: MIL-53 or $Cr^{III}(OH)\cdot\{O_2C-C_6H_4-CO_2\}\cdot\{HO_2C-C_6H_4-CO_2H\}_x\cdot H_2O_y$. J. Am. Chem. Soc. **124**, 13519–13526 (2002)
53. P. Waribam, T.R. Katugampalage, P. Opaprakasit, C. Ratanatawanate, W. Chooaksorn, L.P. Wang, C.-H. Liu, P. Sreearunothai, Upcycling plastic waste: rapid aqueous depolymerization of PET and simultaneous growth of highly defective UiO-66 metal-organic framework with enhanced CO_2 capture via one-pot synthesis. Chem. Eng. J. **473**, 145349 (2023)
54. H.R. Abid, M.R. Azhar, S. Iglauer, Z.H. Rada, A. Al-Yaseri, A. Keshavarz, Physicochemical characterization of metal organic framework materials: a mini review. Heliyon **10**, e23840 (2024)
55. M. Sánchez-Sánchez, N. Getachew, K. Díaz, M. Díaz-García, Y. Chebude, I. Díaz, Synthesis of metal–organic frameworks in water at room temperature: salts as linker sources. Green. Chem. **17**, 1500–1509 (2015)
56. S. Iwaya, H. Konno, One-step facile synthesis of polyethylene terephthalate–derived metal–organic framework for liquid-phase adsorption of benzophenone-4. Chem. Eng. J. Adv. **16**, 100581 (2023)
57. J. Rouquerol, P. Llewellyn, F. Rouquerol, Is the BET equation applicable to microporous adsorbents? Stud. Surf. Sci. Catal. **160**, 49–56 (2007)
58. J.W. Osterrieth, J. Rampersad, D. Madden, N. Rampal, L. Skoric, B. Connolly, M.D. Allendorf, V. Stavila, J.L. Snider, R. Ameloot, How reproducible are surface areas calculated from the BET equation? Adv. Mater. **34**, 2201502 (2022)
59. T. Sun, X. Ren, J. Hu, S. Wang, Expanding pore size of AL-BDC metal–organic frameworks as a way to achieve high adsorption

selectivity for CO_2/CH_4 separation. J. Phys. Chem. C **118**, 15630–15639 (2014)
60. X. Deng, J. Li, B. Zhao, Z. Li, Design of a novel Ag-MOF@ GO composite with a high specific surface area and structural stability for the efficient removal of malachite green. New J. Chem. **47**, 16022–16029 (2023)
61. Y. Zhang, B. Gikonyo, H. Khodja, M. Gauthier, E. Foy, B. Goetz, C. Serre, S. Coste Leconte, V. Pimenta, S. Surblé, MIL-53 metal–organic framework as a flexible cathode for lithium-oxygen batteries. Materials **14**, 4618 (2021)
62. J. Rouquerol, D. Avnir, C. Fairbridge, D. Everett, J. Haynes, N. Pernicone, J. Ramsay, K. Sing, K. Unger, Physical and biophysical chemistry division commission on colloid and surface chemistry including catalysis. Pure Appl. Chem. **66**, 1739e1758 (1994)
63. J. Haber, Manual on catalyst characterization (recommendations 1991). Pure Appl. Chem. **63**, 1227–1246 (1991)
64. P. Holister, C.R. Vas, T. Harper, Nanoporous materials. Technol. White Paper **5**, (2003)
65. F.-G. Li, C. Liu, D. Yuan, F. Dai, R. Wang, Z. Wang, X. Lu, D. Sun, Ultrahigh hydrogen uptake in an interpenetrated Zn4O-based metal–organic framework. CCS Chem. **4**, 832–837 (2022)
66. I. Senkovska, V. Bon, A. Mosberger, Y. Wang, S. Kaskel, Adsorption and separation by flexible MOFs. Adv. Mater. (2025). https://doi.org/10.1002/adma.202414724
67. X. Zhang, R.B. Lin, J. Wang, B. Wang, B. Liang, T. Yildirim, J. Zhang, W. Zhou, B. Chen, Optimization of the pore structures of MOFs for record high hydrogen volumetric working capacity. Adv. Mater. **32**, 1907995 (2020)
68. J. Letwaba, U.O. Uyor, M.L. Mavhungu, N.O. Achuka, P.A. Popoola, A review on MOFs synthesis and effect of their structural characteristics for hydrogen adsorption. RSC Adv. **14**, 14233–14253 (2024)

Publisher's Note Springer Nature remains neutral with regard to jurisdictional claims in published maps and institutional affiliations.